Supplement of Geosci. Model Dev., 15, 5107–5126, 2022
https://doi.org/10.5194/gmd-15-5107-2022-supplement

Geoscientific Model Development
Open Access

Supplement of

The impact of hurricane disturbances on a tropical forest: implementing a palm plant functional type and hurricane disturbance module in ED2-HuDi V1.0

Jiaying Zhang et al.

Correspondence to: Jiaying Zhang (jiaying.zhang@gatech.edu) and Rafael L. Bras (rlbras@gatech.edu)

S1: Outliers of the Height-DBH pairs

To estimate the height-DBH relationship, we chose the height-DBH pairs of stems in the pre-Hugo 1989 census and height-DBH pairs of stems from other censuses with no damage reported to height, based on the census data at Bisley Experimental Watersheds between 1989 and 2014 (Zhang et al. 2022a). Previous studies have shown that using raw data can result in biases in allometric parameters due to the preponderance of small diameter stems and have proposed the use of binned data to give equal weights to each diameter bin (Brown et al. 1989, Duncanson et al. 2015, Jucker et al. 2017). However, we found that the binned data increase the weights for bins with few height-diameter data pairs, such as those in >50cm-diameter bins in Figure S16. Moreover, we found that biases in the height-diameter allometry come from outliers that significantly deviate from the means and are not probable. Therefore, we consider height-diameter data pairs that are outside the plus or minus 1.5 times the standard deviation range, of both the expected height of the diameter bin and the expected diameter of the height bin, as outliers (Figure S16). Specifically, to identify outliers of height-diameter pairs, we divided diameter and height into bins at intervals of 5 cm and 5 m, respectively. For each diameter bin, we first get all the height data in the bin. If there are enough samples (≥10), then we calculate the mean μ and the standard deviation σ of the samples, the points that are outside of the $\mu \pm 1.5\sigma$ range are treated as outliers of height in the diameter bin (green dots). We repeated the same process for the height bins (blue dots). Finally, if a sample point is considered as an outlier in both the diameter bin and the height bin, then this point is considered as an outlier of the height-diameter pairs (red dots) (Figure S16). If there are less than 10 samples in either a height or a diameter bin, then all the data related to those bins are considered insufficient to be used in the estimation of the allometric relationship.

S2: Estimation of hurricane wind speed at BEW

Hurricane wind field can be reconstructed using the HURRECON model, which estimates sustained wind speed, peak gust, and wind direction at a given point using the information of the track, size, and intensity of a hurricane and the cover type (land or water) of the point (Boose et al. 1994; Boose et al. 2004). The sustained wind speed (V_s; m s^{-1}) at any point P in the northern hemisphere are estimated as

$$V_s = F\left[V_m - \frac{1}{2}S(1-\sin(T))V_h\right] \times \sqrt{\left(\frac{R_m}{R}\right)^B \exp\left(1-\left(\frac{R_m}{R}\right)^B\right)}, \qquad \text{(S1)}$$

where F is the scaling parameter for friction (F = 1 if point P is on water, 0.8 otherwise), S is the scaling parameter for hurricane asymmetry (1.0), V_m is the maximum overwater sustained wind speed (m s^{-1}) of the hurricane, T is the clockwise angle (degree) between the direction of the hurricane movement and the direction from hurricane center to point P, V_h is the velocity (m s^{-1}) of the hurricane movement, R is the distance (km) from hurricane center to point P, R_m is the radius of maximum winds (20-80 km), and B is the scaling parameter controlling the shape of the wind profile curve (1.2-1.5).

We estimate the tropical cyclones (39 mph ≤ sustained wind < 73 mph) that passed near BEW within 100 km or hurricanes (≥ 74 mph) that passed within 150 km of BEW between 1989 and 2017 (the period of the BEW censuses) using the HURRECON model. The hurricane best track data HURDAT2 (Landsea and Franklin 2013) are used for parameters F, S, V_m, T, V_h, and R; and we assume that the maximum wind radius Rm = 30 km and the scale parameter of the shape of the wind profile curve B = 1.5 for all tropical storms (cyclones and hurricanes) for convenience.

S3: Estimation of non-photosynthetic vegetation at BEW

Non-photosynthetic vegetation (NPV) data derived from satellite remote sensing retrievals are used to quantify the forest damage from hurricane disturbances. NPV includes exposed wood and surface litter and represents dead vegetation. NPV, together with photosynthetic vegetation (PV, also called green vegetation) and bare soil (BS) are the three main ground cover types. NPV, PV, and BS have distinct spectral reflectance at visible and infrared spectrums, and thus they can be distinguished by satellite sensors with multiple spectral bands. However, satellites cannot distinguish different ground cover types when a grid pixel is a mixture of the three. For each grid pixel, the spectral reflectance measured by satellites (R_λ) is the average of the spectral reflectance of each ground cover type ($M_{type,\lambda}$), weighted by their fractional cover (f_{type}):

$$R_\lambda = f_{NPV} M_{NPV,\lambda} + f_{PV} M_{PV,\lambda} + f_{BS} M_{BS,\lambda}\ , \qquad \text{(S2)}$$

where λ is the wavelength band at which satellite detects signals. The fractional cover of each ground cover type is bounded by two constraints: 1) non-negativity constraint $f_{type} \geq 0$, and 2) sum-to-one constraint $f_{NPV} + f_{PV} + f_{BS} = 1$.

To obtain the fractional cover of each ground cover type, we use the surface reflectance data (R_λ) from Landsat satellites from USGS (https://landsat.gsfc.nasa.gov/). Landsat 4 and 5 satellites provide natural color images and surface reflectance at six wavelength bands—three in visible spectrum (0.45-0.52 μm, 0.52-0.60 μm, and 0.63-0.69 μm), one in near infrared spectrum (0.76-0.90 μm), and two in short-wavelength infrared spectrum (1.55-1.75 μm and 2.08-2.35 μm)—from 1982 to 1992 (Landsat 5 continued to operate until 2012 but no data available). Landsat 7 provides the same information since 1999. Landsat 8 (launched in 2013) provides the same information since 2015 but with slightly narrower ranges of each band (0.45-0.515 μm, 0.525-0.60 μm, 0.63-0.68 μm, 0.845-0.885 μm, 1.56-1.66 μm, and 2.1-2.3 μm). The surface reflectance data have a 30-m spatial resolution and a 16-day temporal resolution, but cloud cover significantly reduces the availability of high-quality surface reflectance data.

The spectral reflectance of the three ground covers ($M_{type,\lambda}$) are derived from the satellite surface reflectance at each spectral band for three boxed areas in Puerto Rico on June 6 and October 12, 2017 (Figure S17). The three boxed areas correspond to dense forest, disturbed forest, and bare ground according to the natural color images from Landsat satellites (Figure S17) and thus represent the ground cover types of PV, NPV, and BS, respectively. The spectral reflectance of the three ground cover types generally agrees with previous results (Yang et al. 2012; Li et al. 2017). It shows that bare soil has the largest reflectance at all the six wavelength bands compared with NPV and PV. PV has a large reflectance on the near infrared (~0.84μm) band but small reflectance on visible (0.4–0.7μm) and short-wavelength infrared (~1.65μm and ~2.21μm) bands.

To obtain the fractional cover of each type (f_{type}), we use the bounded variable least square method following Lawson and Hanson (1974) and Guerschman et al. (2015). Equation (S2) changes to

$$[\boldsymbol{R}, \delta] = \boldsymbol{f}[\boldsymbol{M}, \delta \boldsymbol{1}^m]\ , \tag{S3}$$

where $\boldsymbol{R}$ is a $1 \times n$ dimensional vector of satellite reflectance and n is number of wavelength bands (n=6), $\boldsymbol{f}$ is a $1 \times m$ dimensional vector of the fractional cover and m is the number of ground cover types (m=3), $\boldsymbol{M}$ is an $m \times n$ dimensional matrix of the spectral reflectance of each ground cover type, and δ is a weighting for the sum-to-one constraint and $\mathbf{1}^m$ is the $m \times 1$ vector with all elements being 1. The value of δ is set to 0.2 following Guerschman et al. (2015). Then the fractional cover $\boldsymbol{f}$ is obtained as

$$\boldsymbol{f} = \min_{\boldsymbol{f}} \|\boldsymbol{f}[\boldsymbol{M}, \delta \boldsymbol{1}^m] - [\boldsymbol{R}, \delta]\|_2^2\ , \text{where } \boldsymbol{f} \geq 0\ , \tag{S4}$$

using the embedded function *lsqnonneg* in MATLAB. Thus, the fractional cover of NPV (f_{NPV}) for Puerto Rico is obtained whenever surface reflectance data are available.

ΔNPV is calculated as the difference of NPV between two dates, one before a hurricane and one after the hurricane. The revisit time of Landsat satellites is 16 days, but not all data are available or with high quality because of heavy cloud coverage. Therefore, the pre-hurricane and post-hurricane dates are those closest to the hurricane with high-quality Landsat satellite data (Table S2). The pre-hurricane and post-hurricane dates are usually within a month of the hurricane, and some are three or four months apart. Note that the pre-Hugo date (November 1988) is 10 months before hurricane Hugo (September 1989), the post-Earl date (April 2011) is eight months after hurricane Earl (August 2010), and the dates for hurricanes Marilyn (1995), Bertha (1996), and Georges (1998) are not available because there were no Landsat data available between September 1992 and August 1999. The ΔNPV calculated from two dates, pre- and post-hurricane dates, that are several months apart may be biased and may not reflect the accurate change of NPV from the hurricane due to the seasonal variation of the NPV. Nevertheless, ΔNPV of a hurricane estimated here provides preliminary and approximate information of the mortality of the hurricane.

Figure S18 shows ΔNPV after each hurricane since 1989 with a trajectory close to BEW. Due to heavy cloud coverage, the ΔNPV in many grid pixels is not available. The figure shows that consecutive hurricanes in the same year (i.e., hurricanes Jose and Lenny in 1999, hurricanes Irma and Maria in 2017) caused severer damages (higher ΔNPVs) than a single hurricane. Note that the ΔNPV of hurricane Irene is negative for most of the pixels, indicating decrease of NPV and thus increase of greenness, which is possibly not reflecting the true ΔNPV directly caused by the hurricane. The pre-hurricane date for Irene is April 11 (Table S2), green vegetation could accumulate in the growing season and the fractional coverage of NPV would decrease when hurricane Irene hits on August 22, 2011. Therefore, the NPV before hurricane Irene was possibly overestimated and thus the ΔNPV underestimated.

S4: The relationship between forest mortality and hurricane wind speed

The relationship between the rate of forest mortality and local hurricane wind speed has been studied through an intermediate variable: the fractional coverage of non-photosynthetic vegetation (NPV). The difference of NPV (ΔNPV) before and after a hurricane is indicative of tree mortality. Specifically, negative value indicates decrease of NPV and thus the increase of greenness, positive value indicates increase of NPV and thus mortality, and higher positive ΔNPV indicates higher mortality (Chambers et al. 2007; Negrón-Juárez et al. 2010; Negrón-Juárez et al. 2014). However, the relationship between ΔNPV and wind speed is site sensitive (Chambers et al. 2007; Zeng et al. 2009; Negrón-Juárez et al. 2010; Negrón-Juárez et al. 2014). Therefore, we use ΔNPV to qualitatively represent the forest mortality after hurricane disturbances at BEW.

Figure S19 shows the scatter plot of the average ΔNPV over the 40km × 40km area centered at BEW (blue boxes in Figure S18) after each hurricane against the corresponding wind speed at BEW. It shows ΔNPV is approximately 0.3 after hurricane Hugo and approximately 0.6 after consecutive hurricanes Irma and Maria. Hurricane Irma did not cause direct mortality to the forest, but it removed a significant amount of foliage (Uriarte et al. 2019) and saturated the soils and loosened the roots (Hall et al. 2020), making trees more vulnerable when hurricane Maria came. Thus, we believe the mortality caused by Maria was aggravated because of hurricane Irma. The ΔNPV is around zero for all other hurricanes, which means that those hurricanes do not significantly change the fractional cover of NPV. Therefore, a binary relationship between ΔNPV and local wind speed is suggested:

$$\Delta NPV = \begin{cases} 0, & V < V_0 \\ \Delta NPV_0, & V \geq V_0 \end{cases}. \tag{S5}$$

ΔNPV_0 varies with forest state and other factors. The threshold V_0 is set to 41 m s^{-1} because, based on census data and meteorological records, the largest local wind speed that caused no mortality in BEW is 40 m s^{-1} corresponding to hurricane Georges and the smallest wind speed that caused mortality in the forest is 42 m s^{-1} corresponding to hurricane Maria. Since ΔNPV is indicative of forest mortality (Chambers et al. 2007; Negrón-Juárez et al. 2010; Negrón-Juárez et al. 2014), we assume that hurricane strength has the same binary effect on forest mortality.

Supplementary Tables

Table S1. Values of allometric parameters for each PFT.

Parameter Name	Units	Early	Mid	Late	Palm
H-DBH scale parameter (*a* in Eq. (1))	m cm^{-1}	1.6388	2.2054	2.3833	0.1628
H-DBH shape parameter (*b* in Eq. (1))	-	0.80	0.64	0.59	1.47
Allocation to reproduction	proportion	0.3	0.3	0.3	1
Reproduction min. height	m	18	18	18	18
Minimum height	m	1.5	1.5	1.5	4.8

Table S2. The pre- and post-hurricane dates that are used for calculating ΔNPV for each hurricane. The pre- and post-hurricane dates for Marilyn, Bertha, and Georges are not available because there were no Landsat data in those years. For some hurricanes, the pre- (post-) hurricane dates are months before (after) the hurricane date because there were no high-quality satellite data available for closer dates due to heavy cloud coverage.

Hurricane Name	**Hurricane Date (yyyy-mm-dd)**	**Pre-hurricane date**	**Post-hurricane date**
Hugo	1989-09-18	1988-11-05	1989-10-07
Marilyn	1995-09-16	---	---
Bertha	1996-07-08	---	---
Georges	1998-09-21	---	---
Jose & Lenny	1999-10-21 1999-11-17	1999-09-17	2000-03-27
Debby	2000-08-22	2000-08-02	2001-01-09
Dean	2001-08-22	2001-07-20	2002-04-02
Jeanne	2004-09-15	2004-08-29	2004-10-16
Olga	2007-12-11	2007-09-23	2008-02-14
Earl	2010-08-31	2010-05-10	2011-04-11
Irene	2011-08-22	2011-04-11	2011-09-02
Irma & Maria	2017-09-07 2017-09-20	2017-06-06	2017-10-12

Supplementary Figures

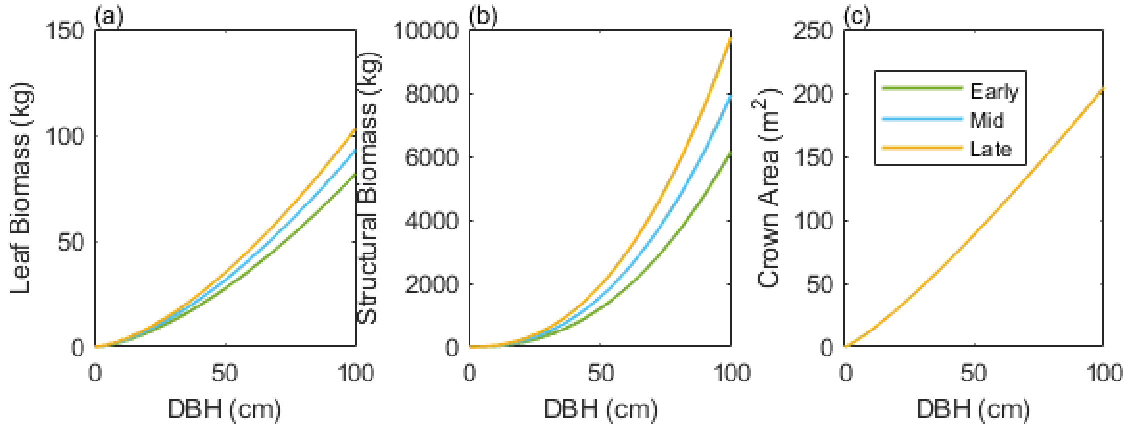

Figure S1. The ED2 model default allometries for each PFT (Early, Mid, and Late tropical successional trees). (a) Leaf biomass-DBH allometry, (b) structural biomass-DBH allometry, and (c) crown area-DBH allometry. The allometries for Palm PFT are assumed to be the same as those for Early PFT.

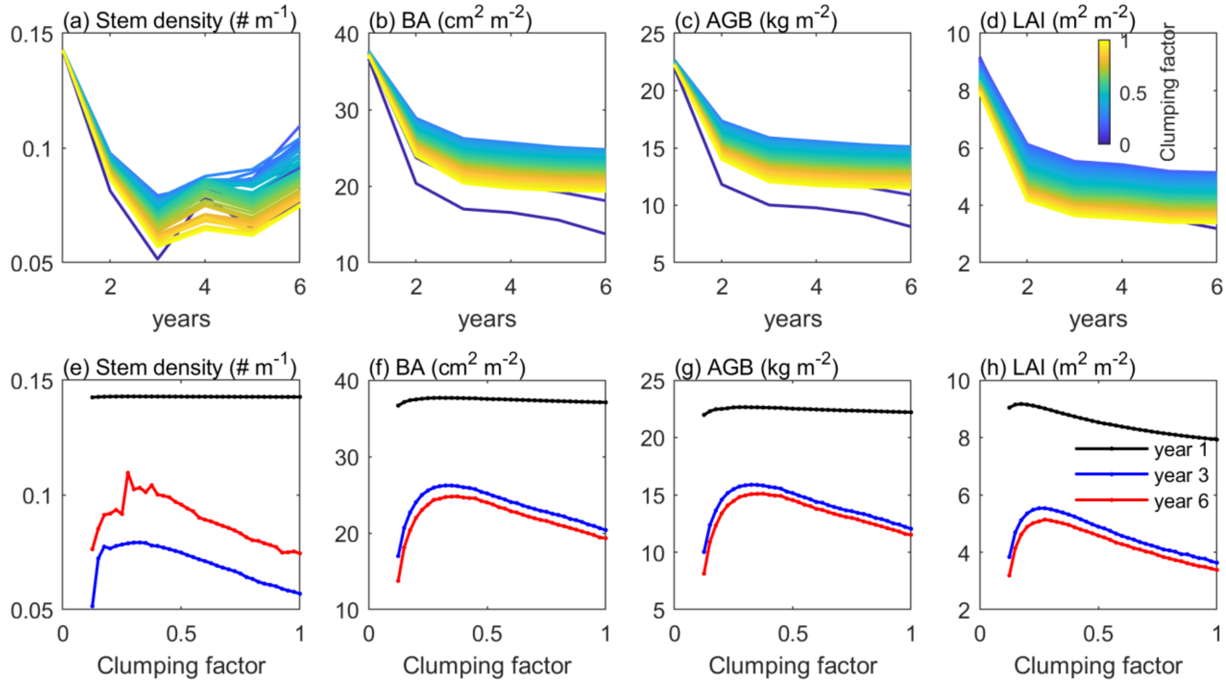

Figure S2. Time series of (a) stem density, (b) basal area, (c) aboveground biomass, and (d) leaf area index for different values of the parameter leaf clumping factor. (e)-(h) The values of the variables at the first, third, and sixth simulation years.

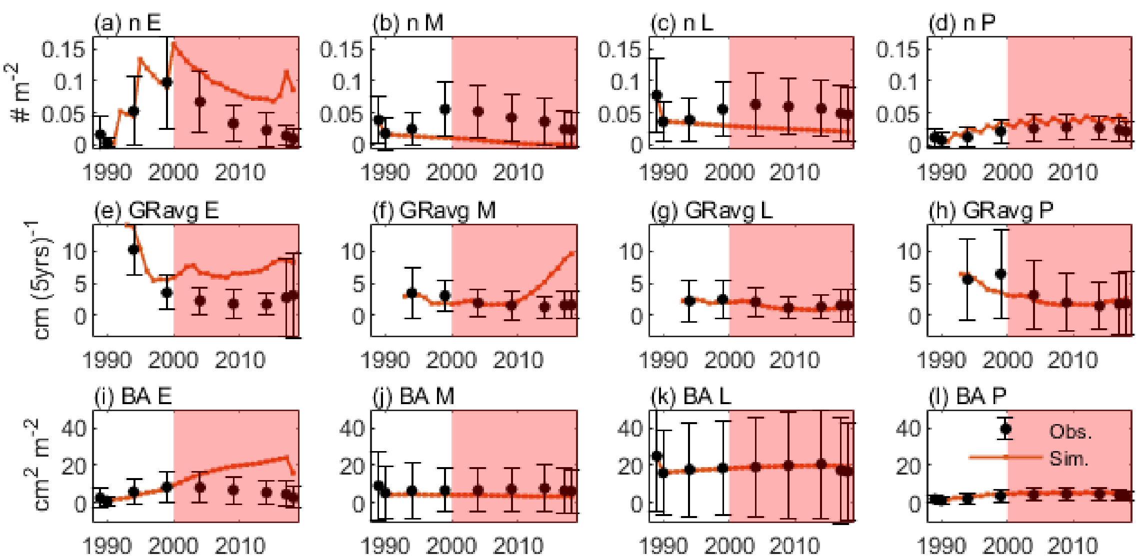

Figure S3. Same as Figure 4, except that the optimal simulations are obtained by training 10 years (1989–1999) instead of 25 years (1989–2014).

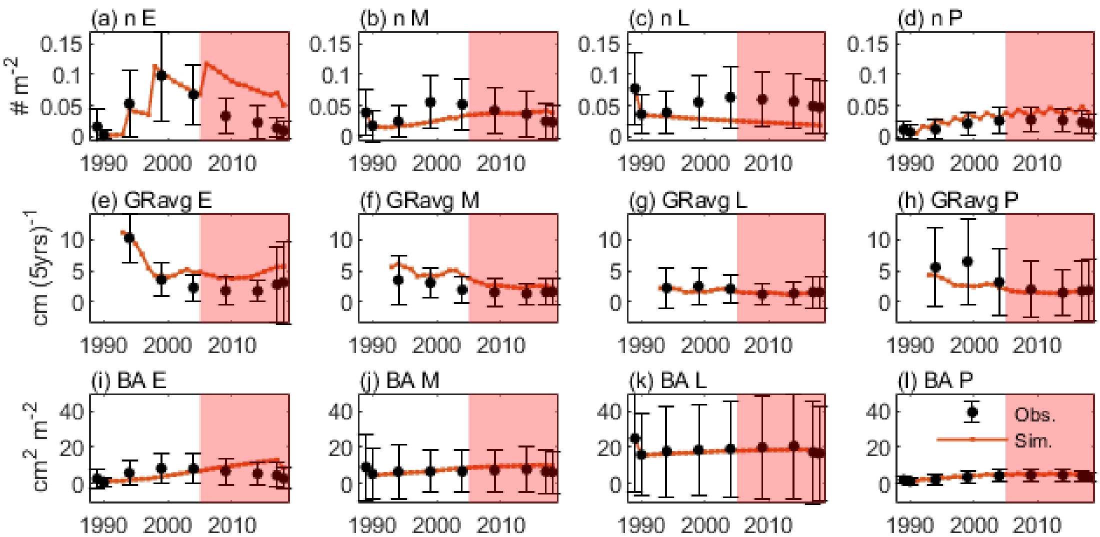

Figure S4. Same as Figure 4, except that the optimal simulations are obtained by training 15 years (1989–2004) instead of 25 years (1989–2014).

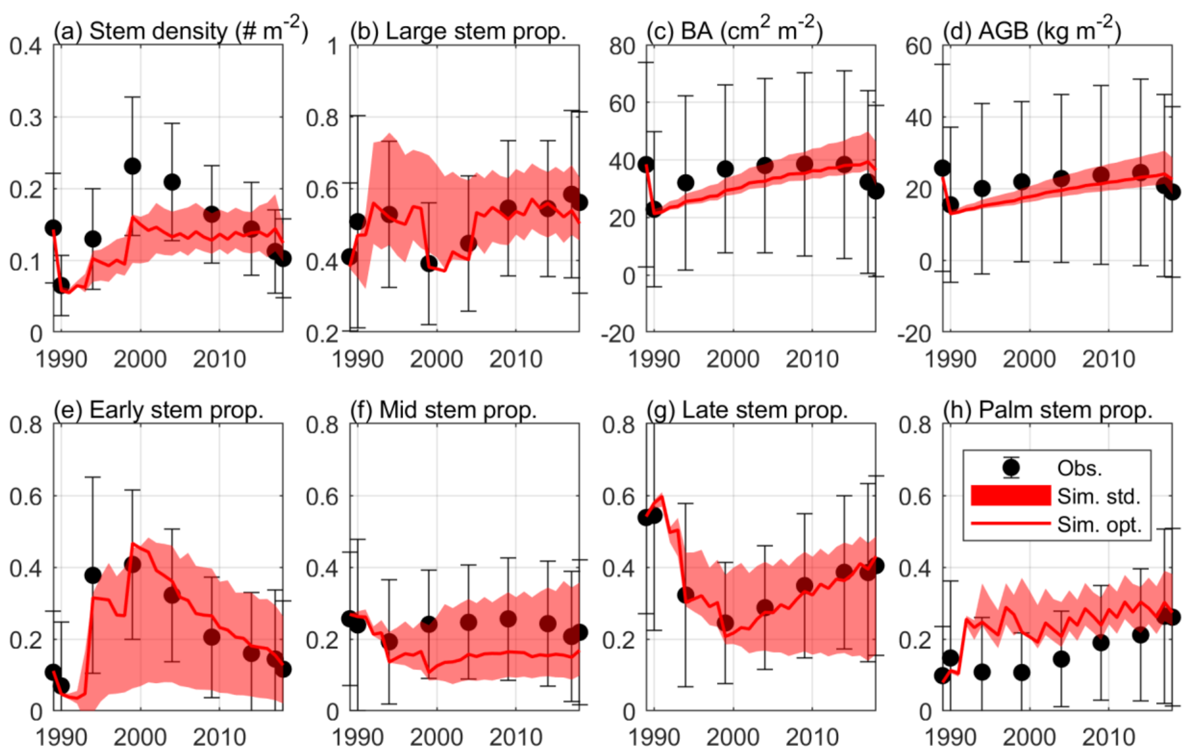

Figure S5. Same as Figure 5, but for K=6.

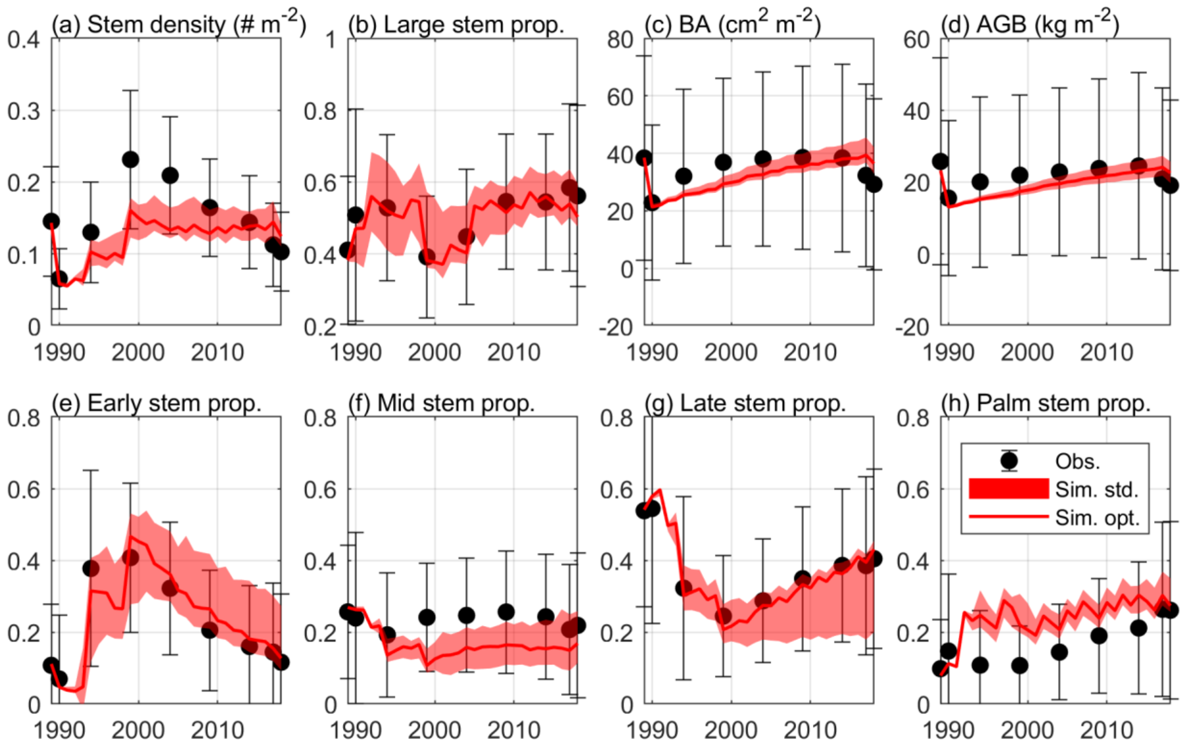

Figure S6. Same as Figure 5, but for K=10.

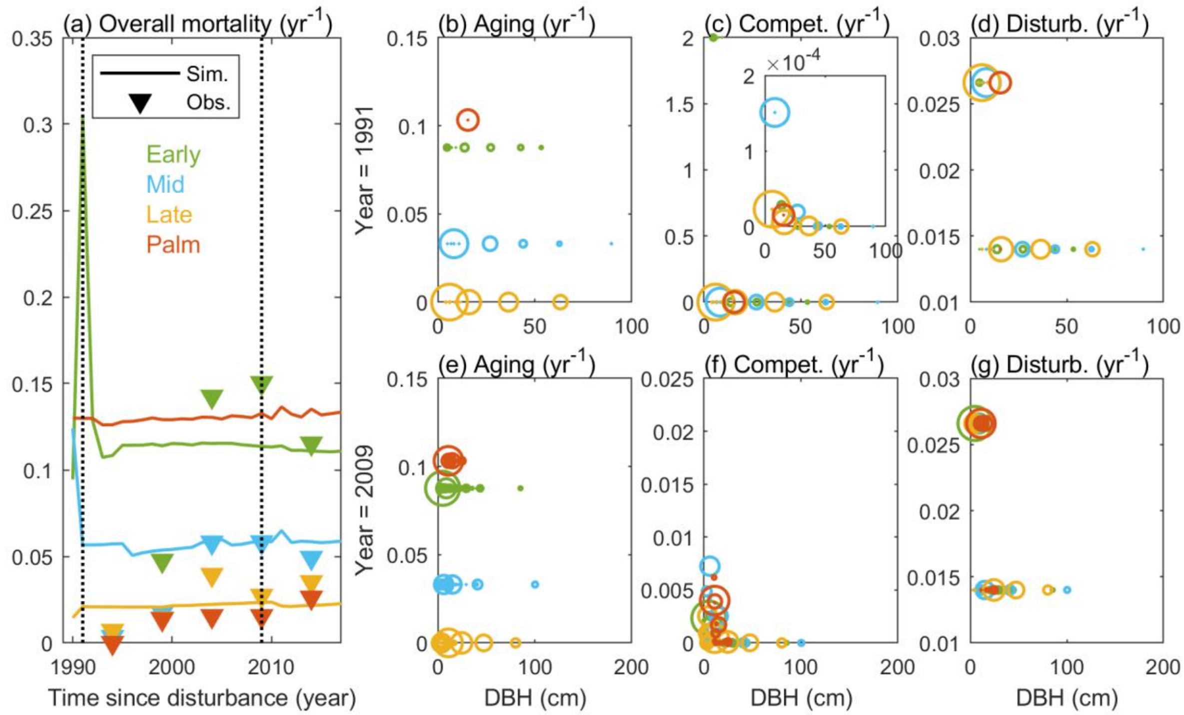

Figure S7. Mortality for each PFT. (a) The time series of the simulated and observed overall mortality for the four PFTs: Early, Mid, Late, and Palm. The simulated mortality from (b) aging, (c) competition, and (d) disturbance for each cohort in year 1991. X-axes are the DBH of the cohort, the color of the circle represents the PFT of the cohort, and the size of the circle is proportional to the density of the cohort (individuals m^{-2}). (e)-(g) are the same as (b)-(d), but for year 2009.

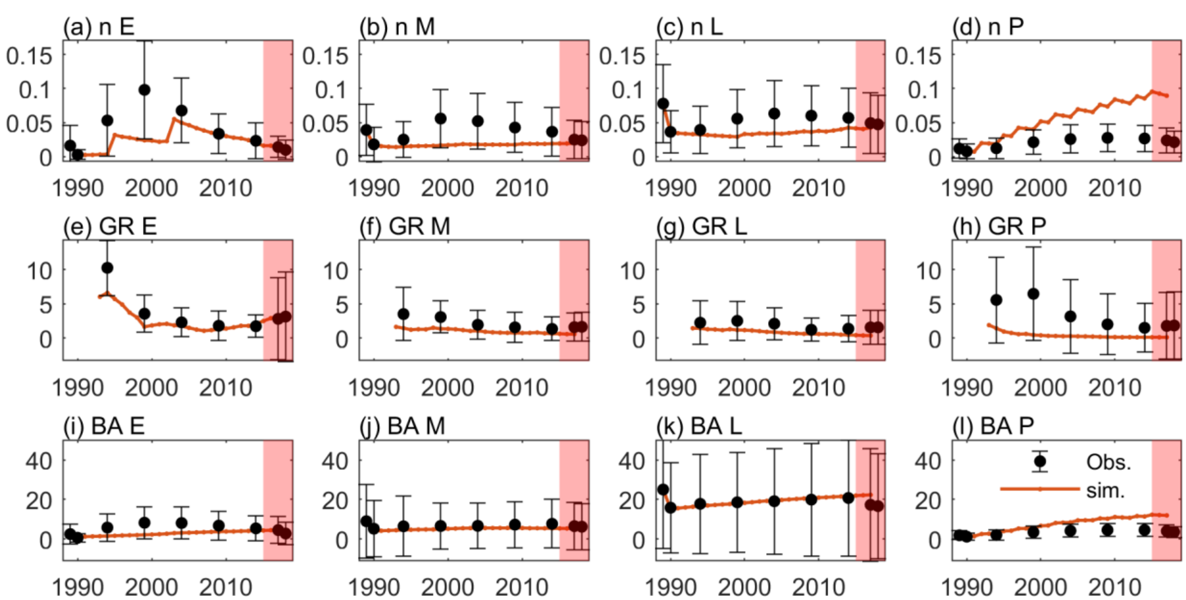

Figure S8. Same as Figure 4, but the model results are from the simulation with the aging mortality of Palm set to zero.

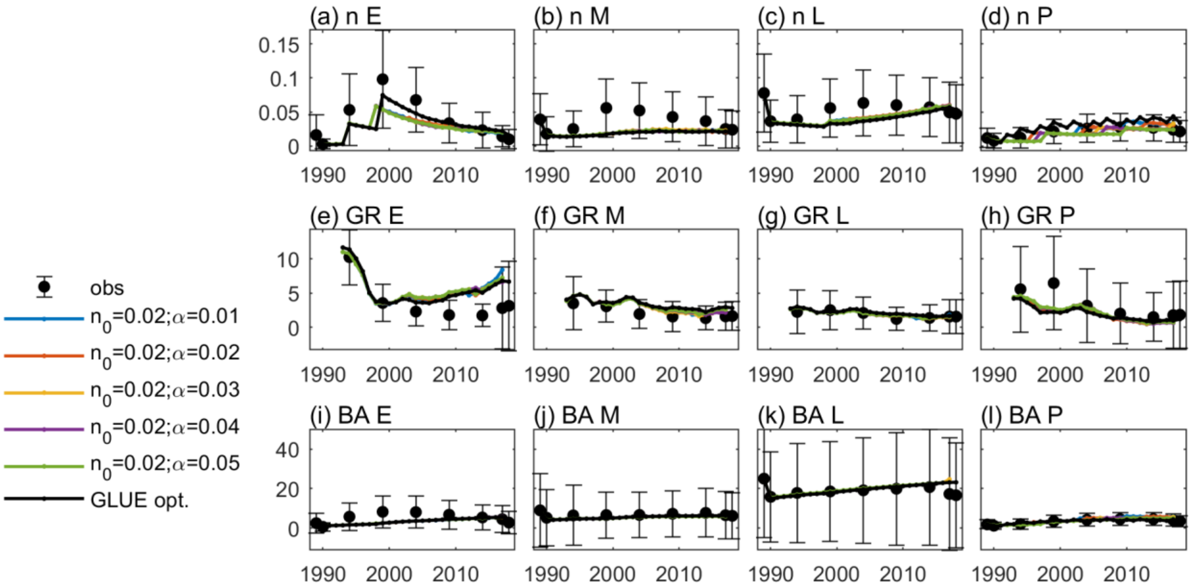

Figure S9. Same as Figure 4, but the optimal simulation is shown in black, and colored lines show experiments with 0 aging mortality and different seedling densities of Palm.

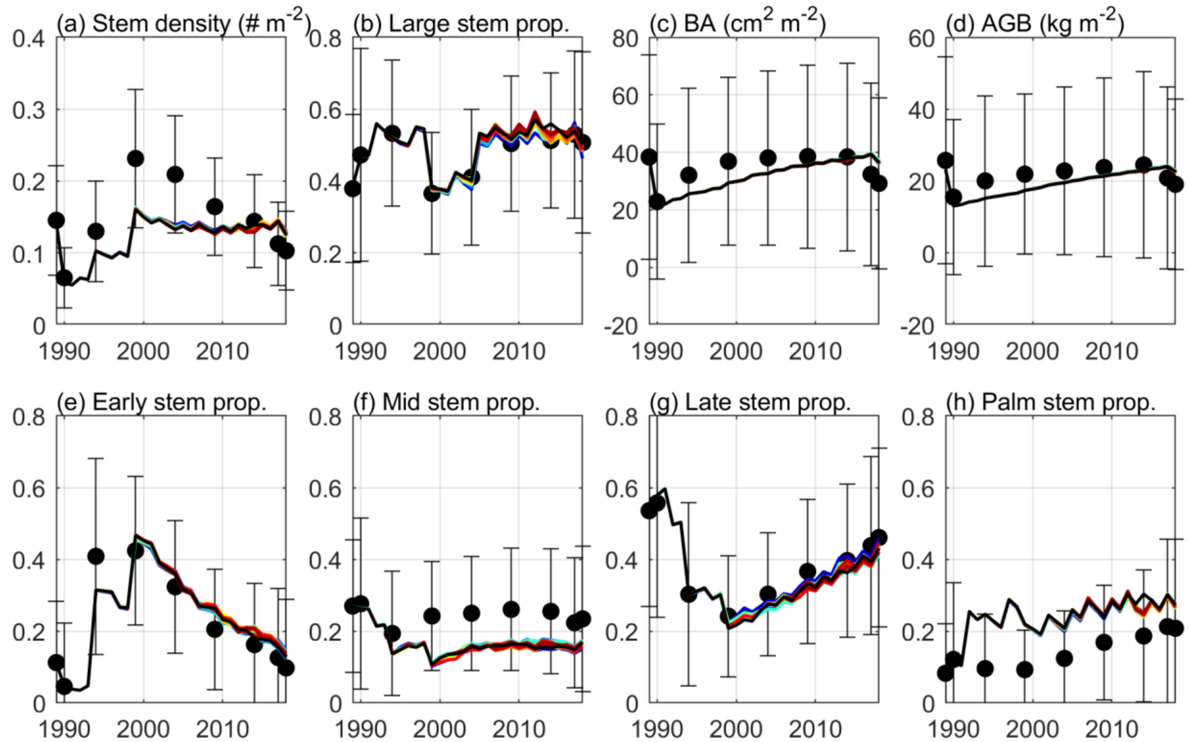

Figure S10. Same as Figure 5, but the optimal simulation is shown in black, and colored lines show the top 20 parameter sensitivity experiments with smaller *MSE* than the optimal simulation.

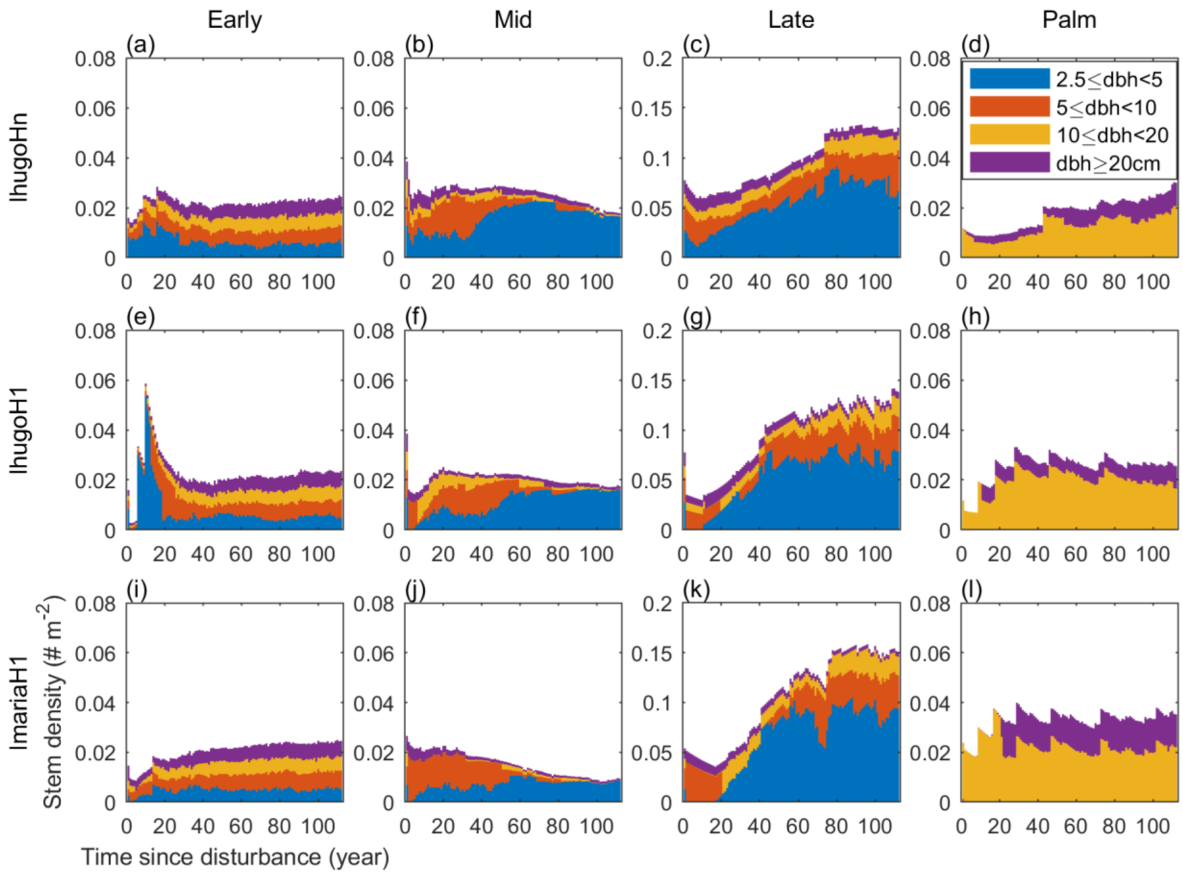

Figure S11. Time series of the distribution of DBHs for the stem density of each PFT from the three experiments.

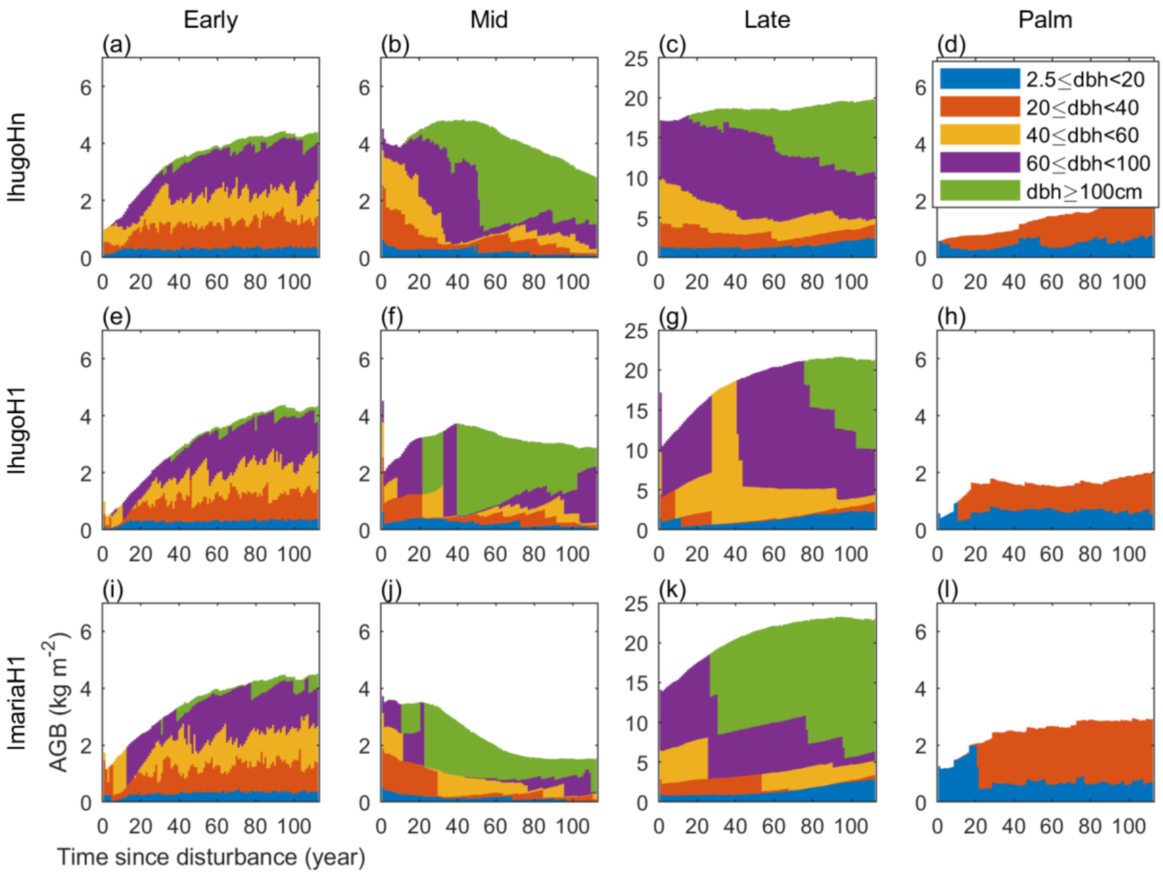

Figure S12. Time series of the distribution of DBHs for AGB of each PFT from the three experiments.

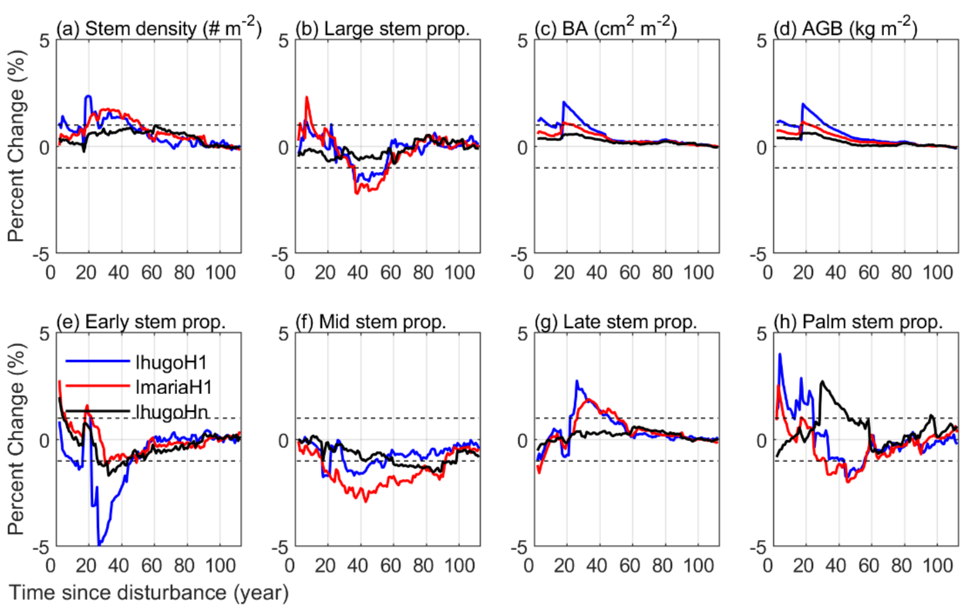

Figure S13. Same as Figure 10, except for the percent change of the 30-year moving average of the variables. The black dashed lines are the −1% and 1% thresholds.

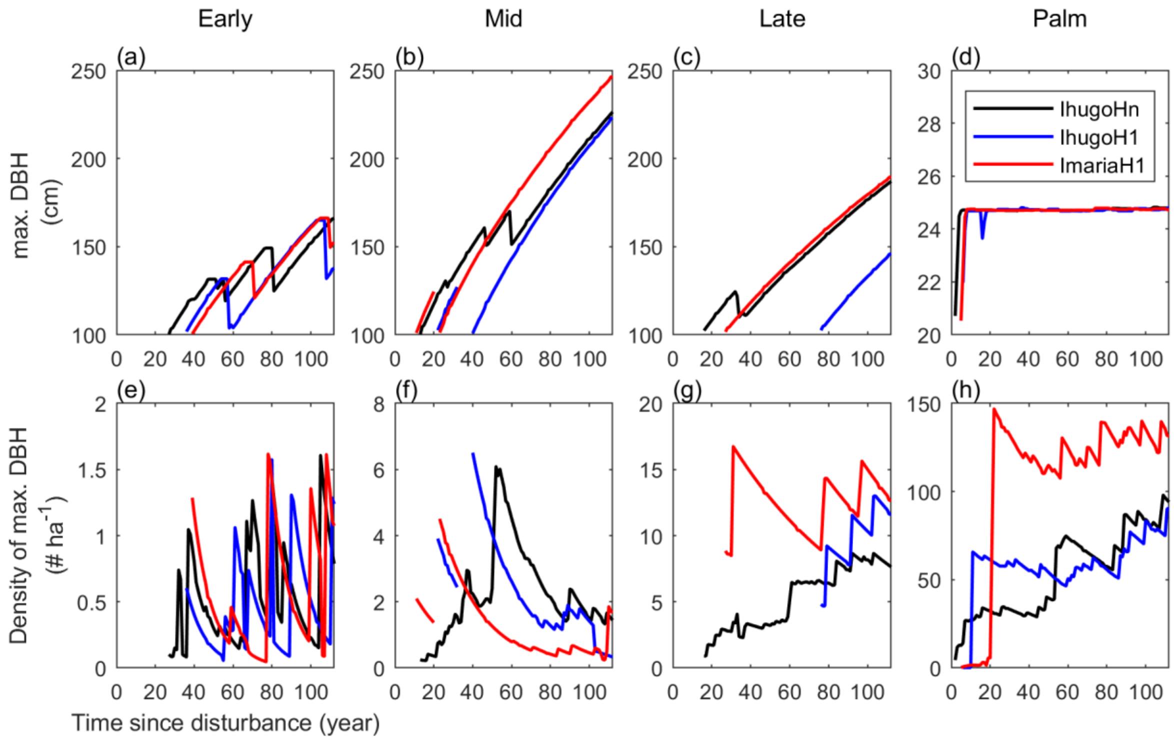

Figure S14. Time series of the maximum DBH and the density of the largest DBH class (DBH ≥ 100 cm for Early, Mid, and Late PFTs, and 20 ≤ DBH < 25 cm for Palm) for each PFT from the three experiments.

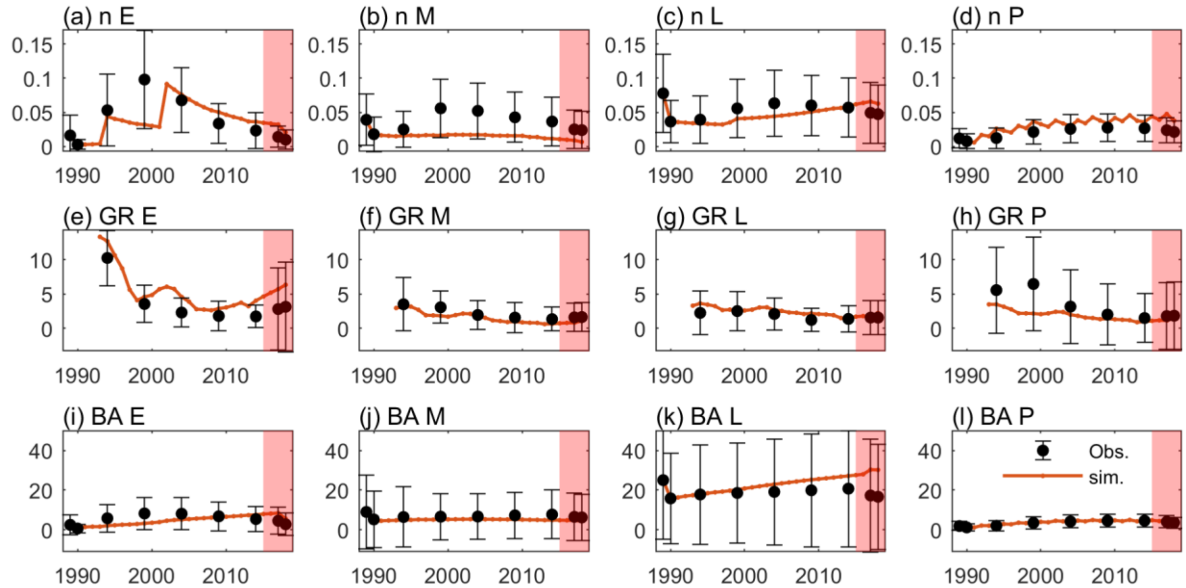

Figure S15. Same as Figure 4, except that the sample size for GLUE is 20,000.

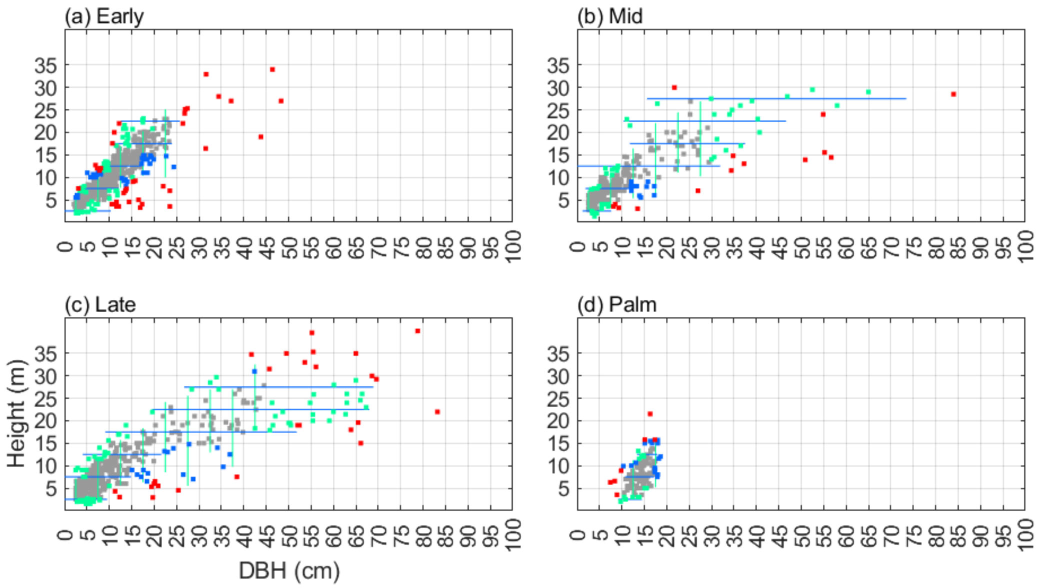

Figure S16. Finding outliers of Height-diameter (DBH) pairs for (a) Early, (b) Mid, (c) Late, and (d) Palm PFTs. DBH and Height were divided into bins with intervals 5 cm and 5 m, respectively. For each DBH (Height) bin, we first get all the Height (DBH) data in the bin. If there are more than 10 samples, then we calculate the mean μ and the standard deviation σ of the samples, get the μ±1.5σ range and mark it as a green (blue) line, and mark the points that are outside of the μ±1.5σ range as outliers with green (blue) dots. If there are less than 10 samples, then all the samples are considered as outliers for this DBH (Height) bin. Finally, if a sample point is marked as an outlier for both the DBH and the Height bins, then this point is considered as an outlier (red dots).

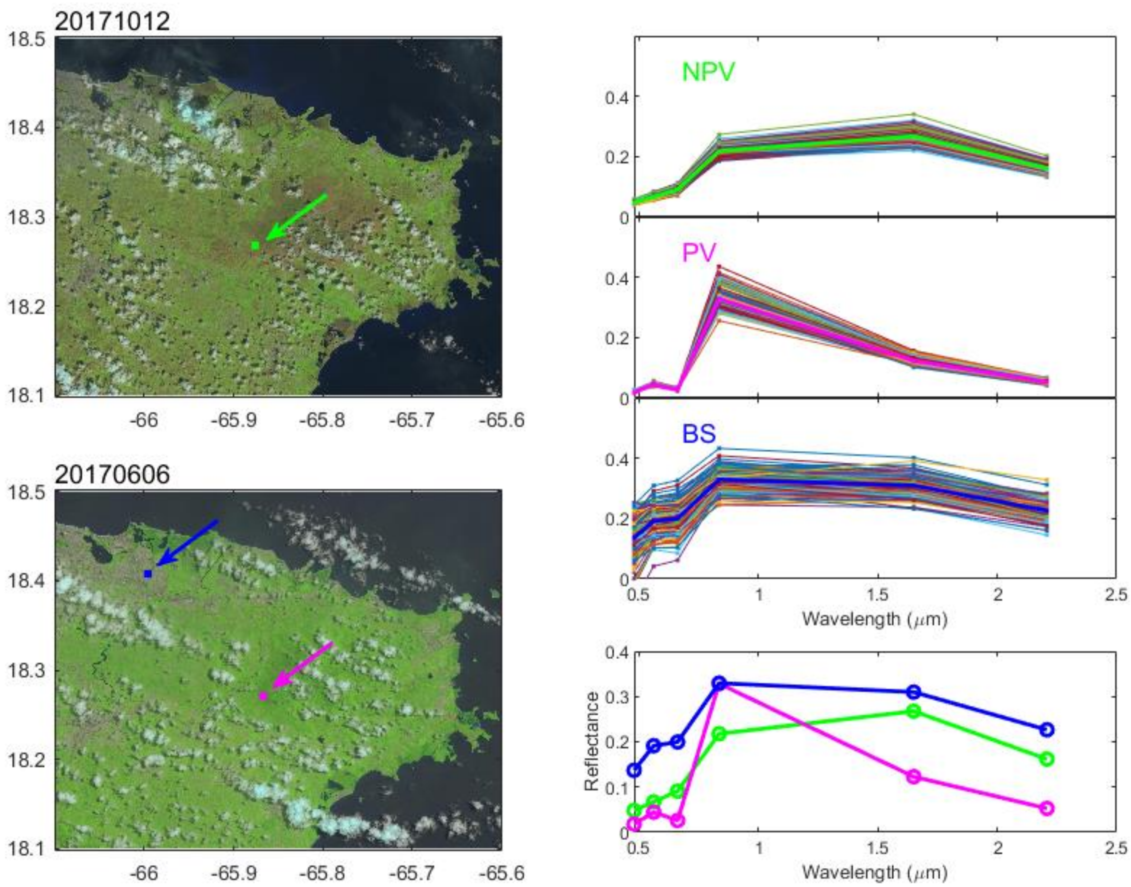

Figure S17. Reflectance of each ground cover type (NPV, PV, and BS) at six wavelengths in the visible and infrared spectrum. The left two panels are the natural color images of two dates. The right panels show the spectral reflectance of the three landcovers. The spectral reflectance of NPV is obtained from the reflectance of a 500m-by-500m spatial domain (about 200 pixels) on October 12, 2017 (green box in the upper left panel), and the those of PV and BS are from the same sized domain on June 6, 2017 (red and blue boxes on the lower left panel).

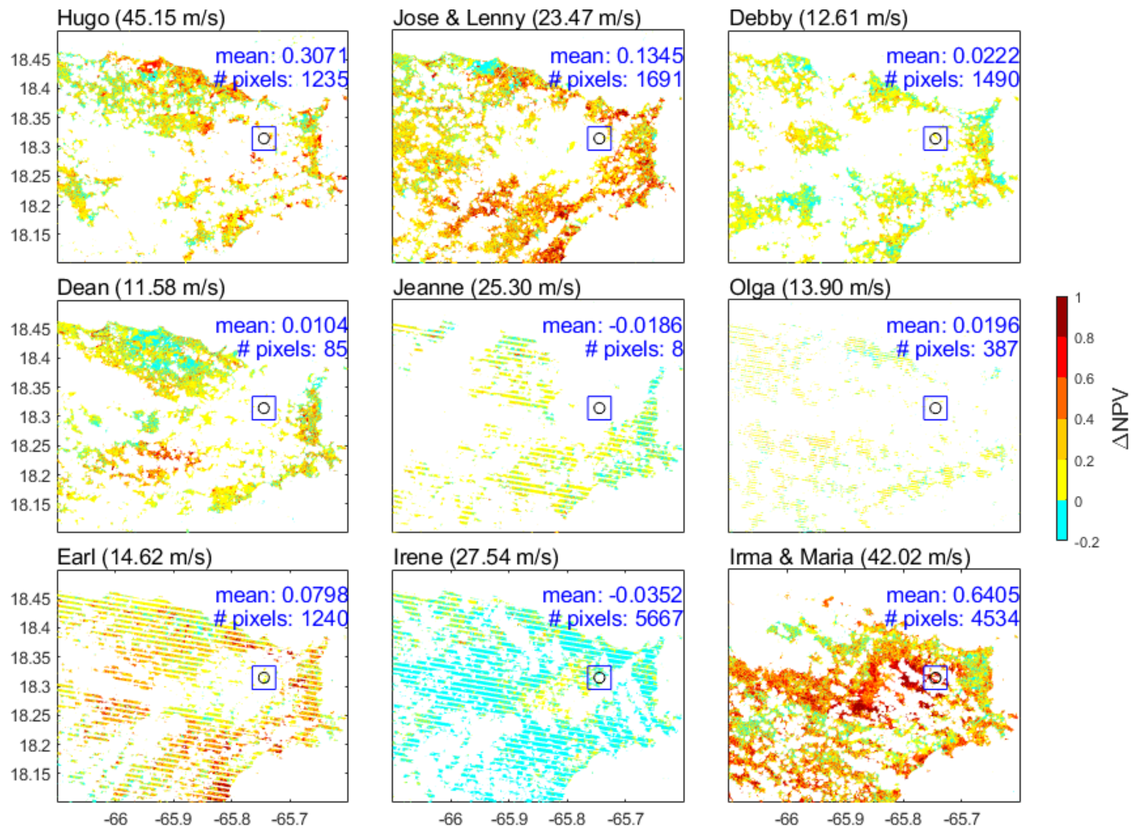

Figure S18. The spatial distribution of ΔNPV over northeastern Puerto Rico for each hurricane. The name of each hurricane and the corresponding maximum wind speed at BEW are shown on the upper left of each panel. The second and the last panels show ΔNPV after two consecutive hurricanes and the wind speed of the stronger one is given in the parenthesis. Pixels over water or covered by clouds are shown in white. The black circle indicates the location of BEW (-65.7449 W; 18.3144 N), and the blue box is a 4km-4km area centered at BEW. The number of pixels inside the box that have ΔNPV value and the mean value of ΔNPV inside the box are shown for each panel.

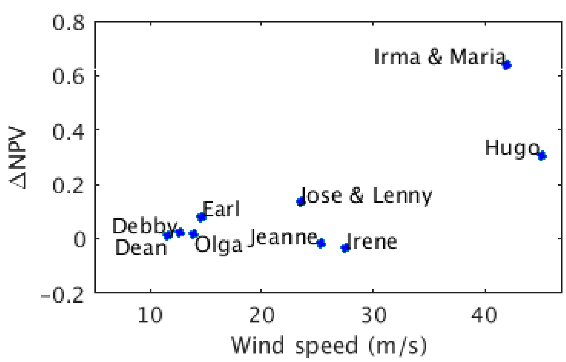

Figure S19. Scatter plot of ΔNPV against the corresponding wind speed at BEW for each hurricane shown in Figure S18.

References

Boose, E. R., Foster, D. R., and Fluet, M.: Hurricane Impacts of tropical and temperate forest landscapes, Ecological Monographs, 64, 369–400, 1994.

Boose, E. R., Serrano, M. I., and Foster, D. R.: Landscape and regional impacts of hurricanes in Puerto Rico, Ecological Monographs, 74, 335–352, 2004.

Brown, S., Gillespie, A. J. R., and Lugo, A. E.: Biomass estimation methods for tropical forests with applications to forest inventory data, Forest Science, 35, 881–902, 1989.

Chamber, J. Q., Fisher, J. I., Zeng, H., Chapman, E. L., Baker, D. B., and Hurtt, G. C.: Hurricane Katrina's carbon footprint on U.S. gulf coast forests, Science, 318, 1107, 2007.

Duncanson, L., Rourke, O., and Dubayah, R.: Small sample sizes yield biased allometric equations in temperate forests, Scientific Reports, 5, 17153, 2015.

Guerschman, J. P. et al.: Assessing the effects of site heterogeneity and soil properties when unmixing photosynthetic vegetation, non-photosynthetic vegetation and bare soil fractions from Landsat and MODIS data, Remote Sensing of Environment, 161, 12–26 2015.

Hall, J., Muscarella, R., Quebbeman, A., Arellano, G., Thompson, J., Zimmerman, J. K., and Uriarte, M.: Hurricane-induced rainfall is a stronger predictor of tropical forest damage in Puerto Rico than maximum wind speeds, Scientific Reports, 10, 4318, 2020.

Jucker, T. et al.: Allometric equations for integrating remote sensing imagery into forest monitoring programmes, Global Change Biology, 23, 177–190, 2017.

Landsea, C. W. and Franklin, J. L.: Atlantic Hurricane Database Uncertainty and Presentation of a New Database Format, Month Weather Review, 141, 3576–3592, 2013.

Lawson, C. L. and Hanson, R. J.: Solving Least-Squares Problems, Upper Saddle River, NJ: Prentice Hall. Chapter 23, p. 161, 1974.

Li, X. et al.: A 2001–2015 Archive of fractional cover of photosynthetic and non-photosynthetic vegetation for Beijing and Tianjin Sandstorm Source Region, Data, 2, 27, 2017.

Negrón-Juárez, R. I. et al.: Widespread amazon forest tree mortality from a single cross-basin squall line event, Geophysical Research Letters, 37, L16701, 2010.

Negrón-Juárez, R., Baker, D. B., Chambers, J. Q., Hurtt, G. C., and Goosem, S.: Multi-scale sensitivity of Landsat and MODIS to forest disturbance associated with tropical cyclones, Remote Sensing of Environment, 140, 679–689, 2014.

Uriarte, M., Thompson, J., and Zimmerman, J. K.: Hurricane Maria tripled stem breaks and doubled tree mortality relative to other major storms, Nature Communications, 10, 1362, 2019.

USGS, 1/3-Arc Second National Elevation Dataset, US Geological Survey, Reston, VA. 2018.

Yang, J., Weisberg, P. J., and Bristow, N. A.: Landsat remote sensing approaches for monitoring long-term tree cover dynamics in semi-arid woodlands: Comparison of vegetation indices and spectral mixture analysis, Remote Sensing of Environment, 119, 62–71, 2012.

Zeng, H., Chambers, J. Q., Negrón-Juárez, R. I., Hurtt, G. C., Baker, D. B., and Powell, M. D.: Impacts of tropical cyclones on U.S. forest tree mortality and carbon flux from 1851 to 2000, Proceedings of the National Academy of Sciences of the United States of America, 106, 7888–7892, 2009.

Zhang, J., Bras, R. L., and Heartsill Scalley, T.: Tree census at Bisley Experimental Watersheds before and after Hurricane Hugo, Fort Collins, CO: Forest Service Research Data Archive. https://doi.org/10.2737/RDS-2022-0025, 2022a.